JOURNAL OF MATERIALS SCIENCE **35** (2000) 5331–5339

Damage threshold velocities for liquid impact

C. F. KENNEDY*, J. E. FIELD
Cavendish Laboratory, Department of Physics, University of Cambridge, Madingley Road, Cambridge CB3 0HE, UK
E-mail: cfk20@cus.cam.ac.uk

Rain erosion is a major cause of strength and transmission loss in IR 'windows' in high velocity flight. The Cavendish Laboratory's Multiple Impact Jet Apparatus (MIJA) is able to simulate high velocity rain impact accurately and reproducibly under laboratory conditions using a series of discrete water jets. Quantitative erosion data in the form of Damage Threshold Velocity (DTV) curves can be obtained, giving the lower limit of damage to the material under study. Damage threshold curves are presented for five different materials carried out using three different nozzle orifice diameters to create the impacting jet. Two approaches are made to predicting the DTV value for each specimen using only data from the standard 0.8 mm nozzle: (i) the 'cylindrical jet' approach, in which the impacting jet is considered to have a flat front, and (ii) the drop ('round-fronted jet') model. Both methods are found to give predictions well within the bounds of experimental error. The former predicts the damage threshold better when the smaller (0.6 mm) nozzle is used and the drop model the threshold when the larger (1.2 mm) nozzle is used. High-speed photographs of jets from differently-sized orifices are presented validating the use of models for the various nozzle diameters. © *2000 Kluwer Academic Publishers*

1. Introduction

Liquid impact (rain erosion) can cause damage to infrared (IR) transmitting 'window' materials during high-speed flight. This damage can result in both strength and transmission losses and it is important to quantify these and understand the basic damage mechanisms. In the early stage of impact, the liquid behaves compressibly and so-called 'water hammer' pressures can be generated. Appendix 1 gives the relevant equations for the pressures and their durations. Studies of liquid impact and the damage produced are most conveniently made by keeping the target stationary and moving the liquid; for a review of techniques, see [1].

1.1. Simulating high-speed liquid impact

The liquid jet technique for simulating drop impact has been developed at the Cavendish Laboratory over the last 40 years. The apparatus initially used was the Single Impact Jet Apparatus (SIJA) designed by Bowden and Brunton [2, 3]. The nozzle design and loading are critical to the success of the technique since it is essential to produce coherent jets with smooth, curved front profiles if they are to simulate drop impacts. Velocities up to ~1200 m/s are routinely achieved. Following the success of SIJA an automated version was developed that would allow greater reproducibility of the jet velocity and contact profile [4–8]. The Multiple Impact Jet Apparatus (MIJA) is shown in Fig. 1. The apparatus consists of a horizontal main pressure vessel with various solenoids and pressure sensors attached. At the top of the main pressures vessel is a firing solenoid, and beneath it a trigger piston blocking a discharge tube leading to the main body. Once the desired firing pressure is achieved in the main pressure vessel the firing solenoid is triggered, and the compressed air allowed to pass down into the vertical main body of the apparatus. This main body houses a piston that can move freely up and down its length. The piston is initially at the top of the main body and on firing it is accelerated down the bore until it comes into contact with the titanium shaft held in the end piece at the lower extent of its travel. Inside this end piece is a bearing that is used to accurately guide the shaft into a nozzle full of water. The specimen is placed below this nozzle on an X-Y-Z stage, and the jet velocity is measured by a series of fibre optics and ultra-fast electronics as it traverses the distance from the nozzle orifice to the specimen. The cycle is finished by clearing the residual water off the specimen surface and then returning the shaft and piston to their initial positions.

The whole operation is controlled by an IBM computer that allows a repetition rate of ~20 impacts/minute. Sites may be positioned with an accuracy of 10 μm on a sample in a random pattern, rectangular grid, or a user-defined array. The major development efforts have been placed into establishing a tight control of the velocities produced (0.5–1%) whilst also ensuring that jet profiles are reproducible and also enabling a velocity measurement system capable of accurately measuring jet velocities of 600 m/s to be fitted into the 20 mm gap between the nozzle orifice and the specimen.

* Author to whom all correspondence should be addressed.

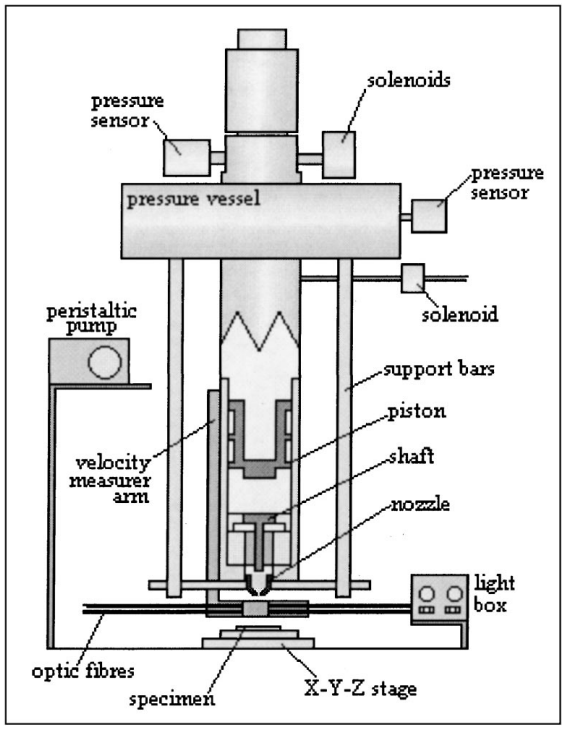

Figure 1 Multiple impact jet apparatus (MIJA).

The damage pattern observed under liquid impact for brittle materials is typically a series of discrete circumferential fractures around the undamaged central loaded zone. The fractures are caused by the Rayleigh surface wave emanating from the impact area [9]. The pressure pulses produced by liquid impact are intense because of the compressible behaviour of the liquid impact in the first stages of impact (see Appendix). An example of damage produced in a brittle material by liquid impact is given in Fig. 2. For further discussion of damage mechanisms, see [2, 9, 10].

A material's rain erosion resistance is characterized by determining its absolute damage threshold velocity (ADTV). This is the velocity below which, for a given water drop size, the sample will not experience any damage regardless of the number of impacts to which it is exposed. Because of the high accuracy of the MIJA jet velocity and positioning, this parameter can be simply obtained from a single sample. The sample (typically a 25 mm diameter disc) has up to 15 sites positioned over its surface, each one allocated an impact velocity and sufficiently separated from adjacent sites so that there is no interaction. Each site is initially impacted once and then inspected for damage under a microscope at $\times 200$ magnification. The lowest velocity at which damage is observed after a single impact is recorded as DTV (1 impact) and the sample returned to MIJA so that each site can be impacted again. This process is repeated until a full curve of DTV against number of impacts is obtained. A threshold curve for spinel is given in Fig. 3 and shows that the curve tends to flatten out after typically 50 impacts. The intercept on the velocity axis after 300 impacts (i.e. DTV (300 impacts)) is therefore very close to the ADTV of the material. A single shot threshold (SST) is the velocity at which a single impact just causes damage when viewed at $\times 200$ magnification. The ADTV decreases as the impacting drop or jet diameter increases. This is related to the number and size of flaws which can be sampled and is discussed later. The values quoted in the earlier work are all for a 0.8 mm diameter jet [10]. A more detailed description of the threshold velocity evaluation procedure can be found in [7, 11].

1.2. Motivation

With the ever-broadening range of materials being tested, as well as the improvements in existing material manufacture, velocities outside the current range of MIJA will be required for future erosion testing purposes. The use of different nozzle sizes would increase the range of velocities attainable while maintaining accuracy. Clearly a way of relating data from different nozzles is of vital importance.

The damage caused by MIJA water jets was evaluated and compared to that resulting from impacts with spherical water drops by [12]. These data showed that the diameter of water drop which gives the same damage pattern as a particular diameter water jet depends on the impact velocity. This is because the front of the jet is not a true hemisphere, but slightly flattened, which means that at low velocities the jet gives the damage observed from a large water drop and as the velocity increases the equivalent drop diameter decreases (see Fig. 4).

2. Results

A comparison was sought between the rain erosion damage caused by a standard 0.8 mm nozzle and that due to 0.6 and 1.2 mm nozzles filled to capacity (0.35 ml). Five specimens were chosen: FLIR zinc sulphide, multispectral zinc sulphide, zinc selenide, silicon and calcium aluminate glass. The same side of each sample was used for each test to eliminate any possible errors due to sample batch or processing variations. As a result, some SST values could not be determined, either because the sample under test failed catastrophically (silicon), or there was insufficient space on the specimen (calcium aluminate glass). A summary of the data obtained is given in Table I and the full damage threshold curves plotted in Fig. 5a–e.

All values for the 0.8 mm nozzle are in good agreement with accepted values [11] with the exception of FLIR zinc sulphide. The data obtained from this specimen are low and it is suspected that the sample was of poor quality. Other workers [11] have quoted a value of 120 m/s. For comparison with calcium aluminate glass, the DTV (0.8 mm nozzle) of soda lime glass is also $\sim$192 m/s.

Fig. 6 shows that as the nozzle orifice diameter is increased, the damage threshold for a given material decreases. The trend is not surprising since it is known that larger jets (drops) are more damaging. Data obtained by Rickerby [13] demonstrated that increasing the radius of curvature of the impacting drop or jet decreases the threshold velocity for damage. The water-hammer pressure on the central axis is the same for all

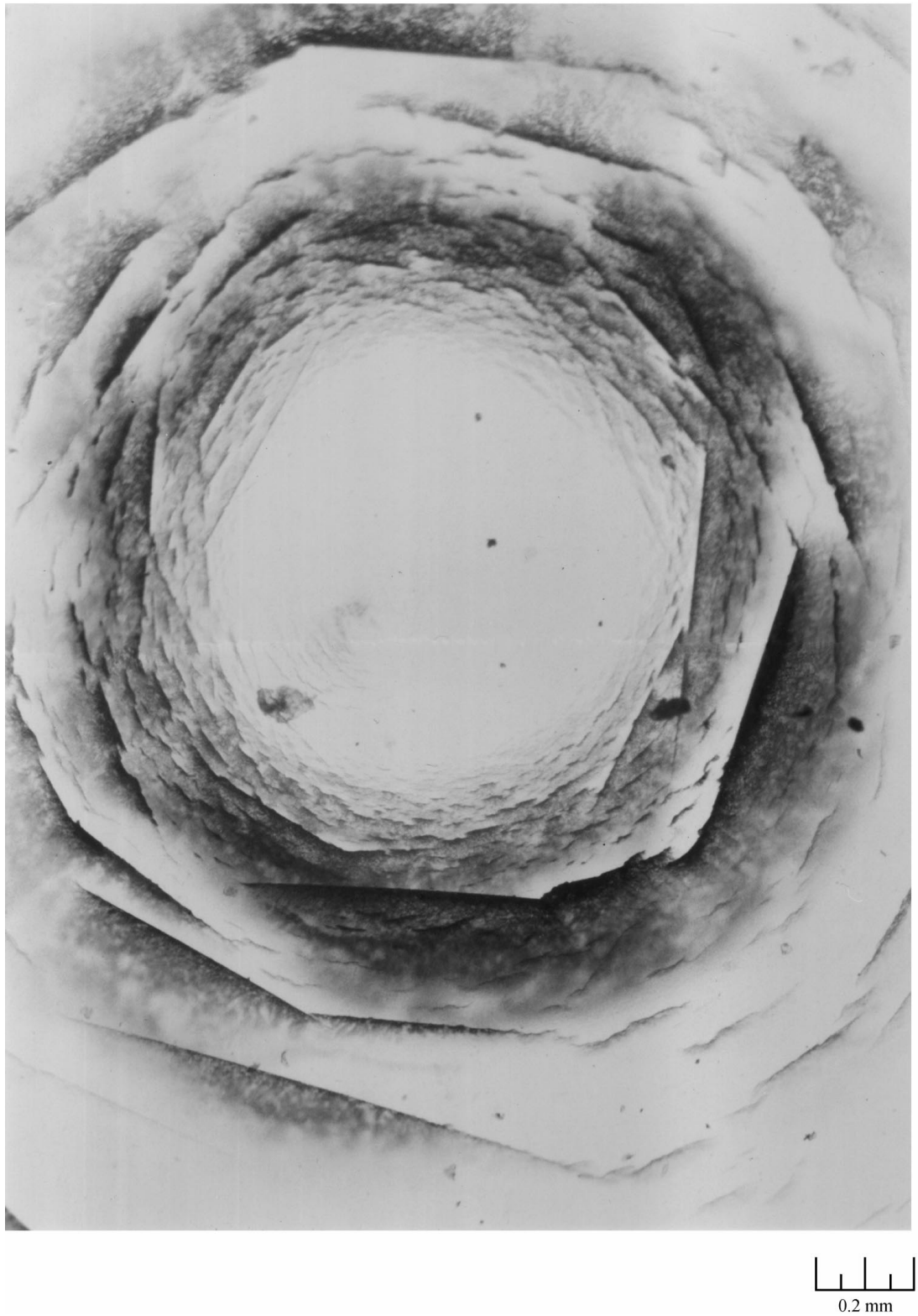

Figure 2 An example of damage in a brittle material resulting from a single liquid impact at 350 m/s.

TABLE I SST and DTV data for five samples using different nozzle orifice diameters; all values ±5 m/s

		0.6 mm nozzle		0.8 mm nozzle		1.2 mm nozzle	
Material	Size, mm	SST	DTV	SST	DTV	SST	DTV
ZnSe	59 × 59 × 12	155	96	140	80	113	67
FLIR ZnS	20 diam. × 3	231	125	186	113	169	110
Multispec. ZnS	25 × 25 × 5	197	116	155	97	140	90
Silicon	25 diam. × 2	356	225	?	196	?	<252
CaAl glass (BS37A)	25 diam. × 5	387	217	?	192	>270	165

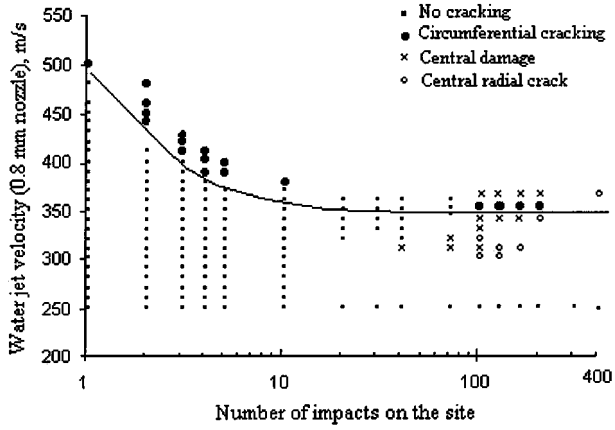

Figure 3 An example of a threshold velocity curve produced by MIJA. This curve is for spinel.

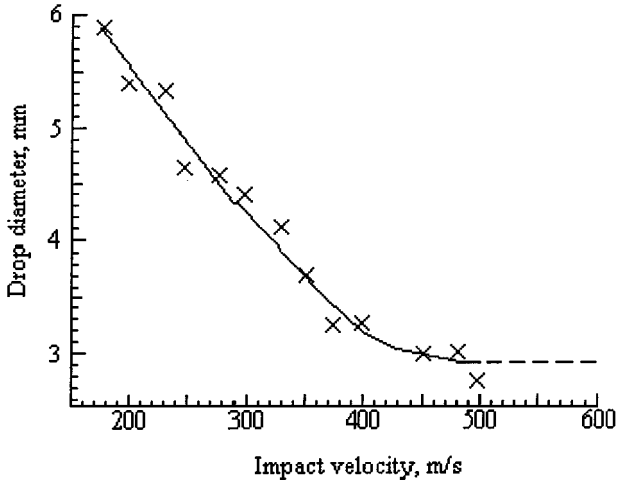

Figure 4 Equivalent drop diameters for 0.8 mm MIJA jet.

drop sizes, so this dependence was attributed to the durations of these initial impact stresses. As the drop size increases, the duration of the impact increases and the severity of the impact also increases. This time duration dependence was quantified by [13, 14, 12] using the damage criteria of Steverding and Lehrigk [15]: $\sigma^2\tau =$ constant. Using Equation A2 (from the appendix) for σ and Equation A5 for τ, this gives

$$V^3 r = \text{constant}. \tag{1}$$

Note that Equation 1 does not involve the shock velocity, C (see [16]).

Increasing the area of the impact has two additional effects. Firstly, the increased duration of the impact will increase the wavelength of the Rayleigh wave and this, in turn, increases the depth to which it penetrates [17]. Since the stress intensity at the crack tip is determined by the integrated stress along the length of the crack, the greater depth of penetration increases the impact severity. Secondly, the increased area over which the stresses act will increase the chances of them encountering a critical flaw. The magnitude of this effect is determined by Weibull statistics (see, for instance, [18]) which shows that for an increase in impacted area from A_1 to A_2, the impact strength will drop by a factor $(A_1/A_2)^{1/m}$, where m is the Weibull modulus, which for the materials of interest in this study is between 2 and 15. Note that Equation 1 is valid for *curved* jets and drops. For ideally cylindrical jets, the duration of the high pressure phase τ_j is shorter and given by

$$\tau_j = \frac{R}{C}. \tag{2}$$

Using the $\sigma^2\tau =$ const relation and incorporating the first order shock correction $C = C_0 + kV$, where C_0 is the acoustic velocity and $k = 2$ for water, the impact velocity and jet radius, R, for *cylindrical jets* are related by

$$V^2 CR = V^2(C_0 + kV)R = \text{constant}. \tag{3}$$

Note that Equation 3 does contain the shock velocity, C [16].

2.1. Worked example

Consider standard DTV data for FLIR zinc sulphide [12] which for a 0.8 mm nozzle is ∼120 m/s. The DTV for a 0.6 mm nozzle may be estimated using the two approaches outlined above. The first approach assumes that the nozzles produce equivalent drops of radii proportional to the orifice radii. Equation 1 predicts a $DTV_{0.6}$ of 132 m/s. Secondly if it is assumed that each nozzle produces flat-fronted jets of radius proportional to the orifice diameter and that $C_0 = 1500$ m/s, then the $DTV_{0.6}$ is 136 m/s. In this case the values of both estimates are close and within experimental error of each other, but this is not necessarily so for other DTVs.

2.2. Predicted DTVS using 0.8 mm DTV data

Similar calculations have been performed for all the materials tested in Table I. Table II summarizes the 0.6 mm

TABLE II Measured DTVs using a 0.6 mm nozzle, compared to the values predicted from 0.8 mm DTVs. Values in bold show which model makes the best prediction for the 0.6 mm jet

Material	Measured 0.8 mm DTV, m/s	Predicted 0.6 mm DTV, m/s		Measured 0.6 mm DTV, m/s
		Jet equation	Drop equation	
ZnSe	80	**91**	88	96
FLIR ZnS (exptl)	113	128	**124**	125
FLIR ZnS (lit.)	120	136	132	—
Multispec. ZnS	97	**110**	107	116
Si	196	**221**	218	225
CaAl glass	192	**216**	211	217

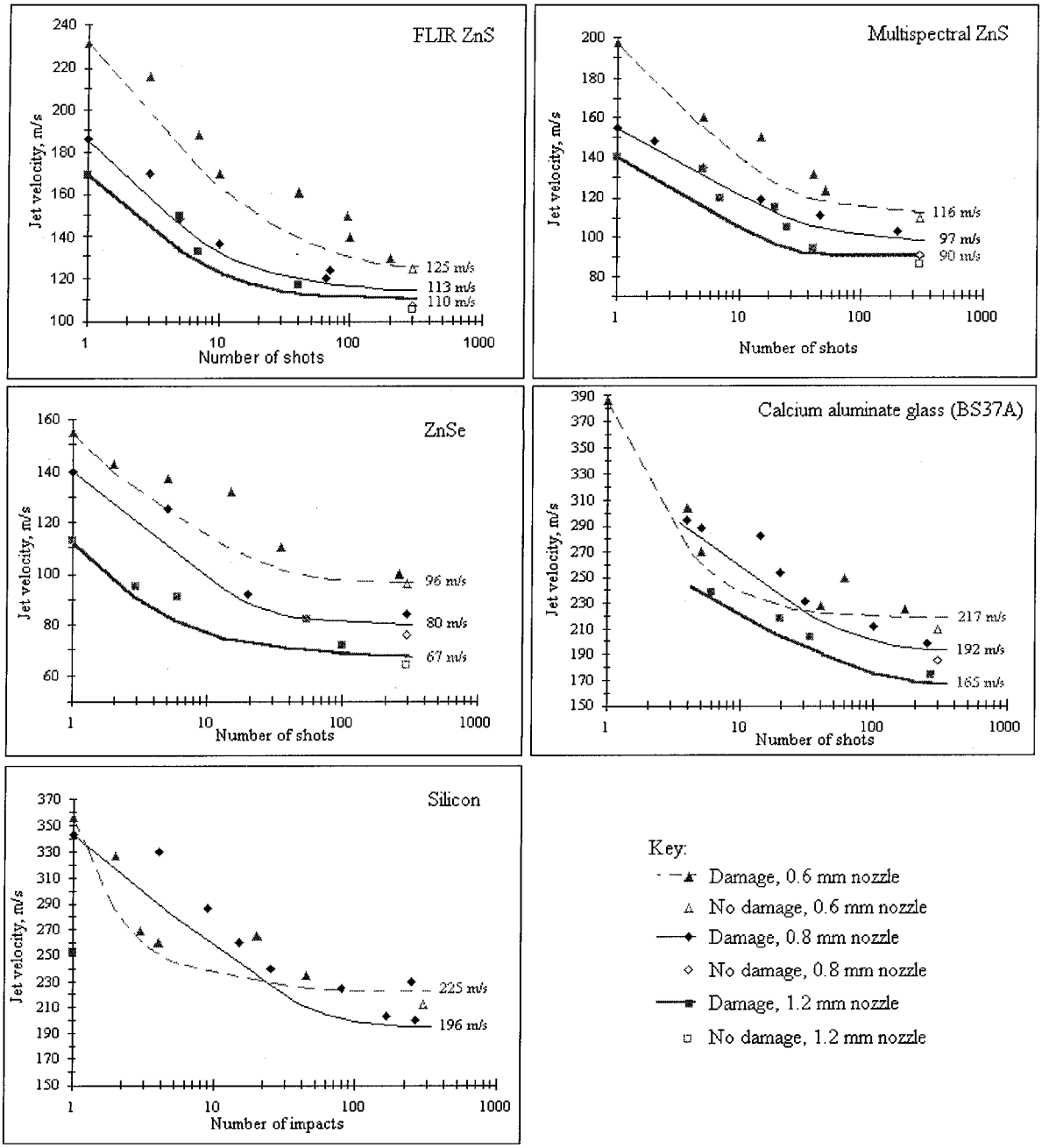

Figure 5 Damage threshold curves for selected specimens (a–e).

DTVs predicted from both the above approaches using data obtained experimentally with a 0.8 mm nozzle. The exercise is repeated in Table III using 0.8 mm DTV data to predict the 1.2 mm DTV. In each case the 'predicted' values assuming the 'jet and 'drop' equations are compared with experimental data obtained in the present study.

Clearly the predictive capability, based on the $\sigma^2\tau =$ constant relation is very good for either jet size. The 'jet' equation is best for the 0.6 mm jet in four out of five instances. For the 1.2 mm DTV prediction, the 'drop' is best (or equally good) in four cases out of five. From the above analysis it is predicted that the jet emerging from a 1.2 mm nozzle orifice filled to capacity will be more rounded than one emerging from a 0.6 mm nozzle. To confirm this, and to provide further support to the models, photographic evidence of the shape of the different jet front profiles was sought.

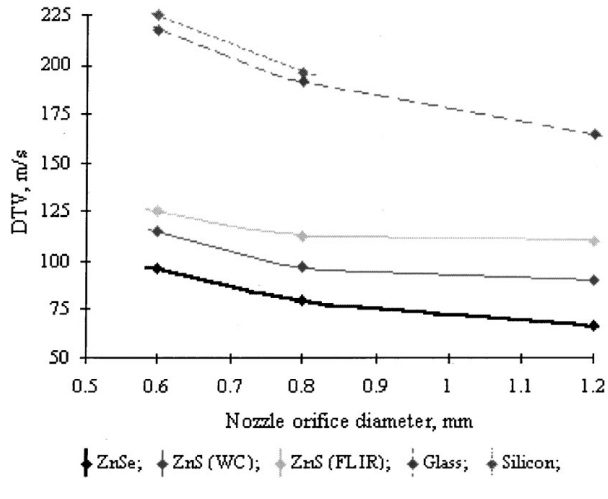

Figure 6 Change in DTV with nozzle size for five different materials.

TABLE III Measured DTVs using a 1.2 mm nozzle, compared to the values predicted from 0.8 mm DTVs. Values in bold show which model gives the best prediction for the 1.2 mm jet. Note that in the case of glass, the models are equally good

Material	Measured 0.8 mm DTV, m/s	Predicted 1.2 mm DTV, m/s		Measured 1.2 mm DTV, m/s
		Jet equation	Drop equation	
ZnSe	80	**66**	70	67
FLIR ZnS (exptl)	113	94	**99**	110
FLIR ZnS (lit.)	120	100	105	—
Multispec. ZnS	97	81	**85**	90
Si	196	165	**171**	<252
CaAl glass	192	**162**	**168**	165

3. High-speed photography

A number of different photographic techniques have been used in high-speed liquid impact studies over the years. For a full review of high-speed photography see Field [19]. Bowden and Brunton [3] used the Cranz-Schardin system, and Bowden and Field [10] and Camus [20] both used a Beckman and Whitley 189 rotating mirror camera. More recently Field and coworkers have used image converter cameras [21, 22, 1]. Rickerby [13] used an Imacon camera and different illumination set-ups to obtain pictures of jets emerging from SIJA. Typically, three types of jets are produced

(a) the traditional well-rounded jet front generated from a convex meniscus at the orifice before firing

(b) Monroe jets, which arise if the meniscus at the orifice before firing is concave;

(c) Jets suffering Taylor instabilities, which may arise when an accelerated liquid is disturbed; they take the form of exponential increasing perturbations [23, 21].

Fig. 7 shows examples of each, reproduced from Rickerby [13]. Only the well-rounded example is of practical use for rain erosion studies.

Compared with SIJA there has been relatively little work on jets produced by MIJA. Clearly it is of vital importance that the jet fronts be coherent and reproducible. These characteristics are strongly suggested by the damage patterns obtained on a wide range of materials.

Three different sizes of orifice were studied (0.6, 1.2 and the standard 0.8 mm diameter), and the velocities kept to within the normal working range of the machine. Unless otherwise stated the water volume in the nozzle is 0.35 ml. An Imacon 792 camera, capable of framing rates of up to 6×10^7 fps, was used to photograph the jet, illuminated by a flash source, both triggered from the uppermost light beam of the velocity measurer via a delay generator. A combination of lenses magnified the subject to approximately $4\times$ its actual size. A series of six frames were captured with an interframe time of 5 μs.

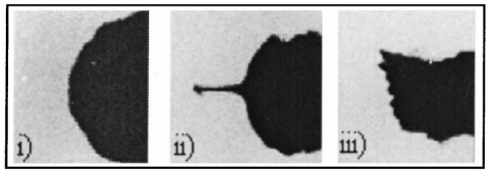

Figure 7 (from [13]): Three types of jet which may emerge from a SIJA nozzle: (i) a well-formed round-fronted jet from a 1.6 mm nozzle travelling at ∼550 m/s; (ii) a Monroe jet from a nozzle 2.4 mm nozzle travelling at ∼280 m/s; (iii) a Taylor instability in a jet travelling at ∼750 m/s from a 0.4 mm nozzle.

Examples of the high speed photographs obtained are given in Fig. 8. A series of up to seven frames have been overlaid to show the progress of the (same) jet travelling approximately 20 mm below the nozzle orifice. The cores of the two larger jets are clearly visible.

It was expected that the 1.2 mm nozzle would produce the most round-fronted jets as a result of the highly convex meniscus formed initially at the orifice, and indeed this was found to be the case. However, the meniscuses formed at all orifices before firing are convex even for the narrowest diameter. It is interesting to note, therefore, the relative flatness of some jet fronts with respect to the 'ideal' geometry used in theoretical predictions. This is especially true of the jet from the 0.6 mm nozzle.

Hand [24] showed that a 0.8 mm jet travelling at 200, 250 and 300 m/s theoretically simulates a drop 2 mm in diameter travelling at velocities 250, 300 and 350 m/s respectively. Indeed this is underlined by the experimental data presented above which, for a jet from a 0.8 mm nozzle, suggest the jet front 20 mm below the nozzle to be in the region 1.75–2.25 mm in diameter.

Fig. 9 shows a schematic of the nozzle. Note there are two volumes of liquid to consider: *A*, water in the water-guide section, and *B*, the much larger volume in the nozzle chamber. Following impact, a shock wave moves through the liquid and when the central part along the axis OO′ reflects off the liquid/air interface, this surface will start moving with a particle velocity $2v$. The other parts of the shock reflect from the inner wall of the orifice and travel to and fro between it and the piston accelerating and overtaking that from *A*. The liquid in *A* is pushed aside and effectively forms the mushroom-head and spray. This explains why the jet front accelerates after emerging from the nozzle and approaches a plateau velocity after 10–20 mm, depending on jet size [25]. For the larger orifice nozzle, the volume of liquid in *A* is larger and the spray cloud is larger. Alternatively, for the smaller orifice (0.6 mm diameter) the spray cloud is reduced and the central flat part is effectively the fast jet core. This is all consistent with the photographic evidence of Fig. 8.

From both the jet front profiles and the damage patterns regularly obtained, MIJA does not produce Monroe jetting or Taylor instabilities. In fact, the

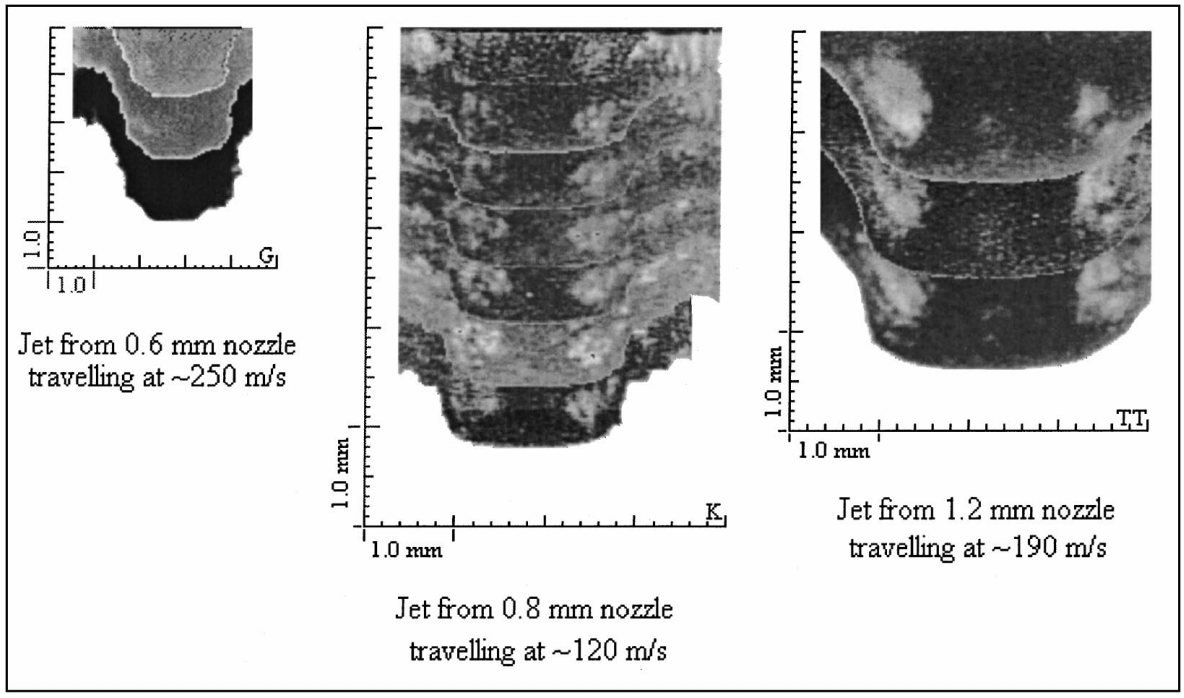

Figure 8 The progress of jets from different nozzles approximately 20 mm below the orifice.

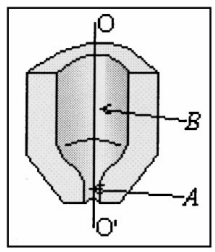

Figure 9 Schematic of a typical MIJA nozzle defining two distinct volumes *A* and *B*.

vertical configuration of MIJA is an advantage since a convex and reproducible meniscus is achieved.

The photographs presented in Fig. 8 show that 'cylindrical' and 'drop' models chosen for the DTV analysis are appropriate.

4. Conclusions

DTV data were obtained for five samples using three different nozzles, namely 0.6, 0.8 and 1.2 mm. Values for the 0.8 mm nozzle compare favourably to data collected by other workers [11]. DTV values for the smaller nozzle for a given material are higher than values from larger nozzles, but this is consistent with the smaller equivalent drop sizes they simulate.

Using the standard 0.8 mm nozzle data two approaches were taken to try to predict the DTV for other nozzle sizes. The 0.6 mm DTV data was found to be most effectively modelled by the 'cylindrical jet' model whilst the 1.2 mm DTV was best predicted by the 'drop' approach.

In general, the profiles of the jets from MIJA V are in agreement with those observed from SIJA and predicted by theory. Unlike SIJA, MIJA has shown that it can create reproducible jets of good quality on demand, with no risk of Monroe jetting or Taylor instabilities. This is underlined by the comprehensive set of photographs presented of the jets in flight.

It is encouraging that, not only do the theoretical predictions confirm the real shape of the different jets, but also that they agree with practical DTV data to within the limits of experimental error. The 0.6 mm nozzle will provide a feasible option when high impact velocities are necessary in future research.

Appendix : Liquid impact

Liquid impact consists of two main stages; initially the liquid behaves in a compressible manner generating the so-called 'water hammer' pressures. These high pressures are responsible for most of the damage resulting from liquid impact and are maintained while the edge of the contact area between the impacting liquid and the solid moves supersonically with respect to the shock speed in the liquid [10, 26–28]. Fig. A1 illustrates the situation a short time after impact.

As pointed out by Lesser [27], it is possible to use Huygen's construction to find the shape of the shock envelope. The pressure on the central axis is given by

$$P_c = \frac{V\rho_1 C_1 \rho_2 C_2}{\rho_1 C_1 + \rho_2 C_2}. \quad \text{(A1)}$$

Where V is the impact velocity and $\rho_1\rho_2$ and C_1, C_2 are the densities and shock velocities of the liquid and the solid, respectively. For impact on a rigid target, the pressure is

$$P_c = r_1 C_1 V. \quad \text{(A2)}$$

frequently referred to as the 'water hammer' pressure [29].

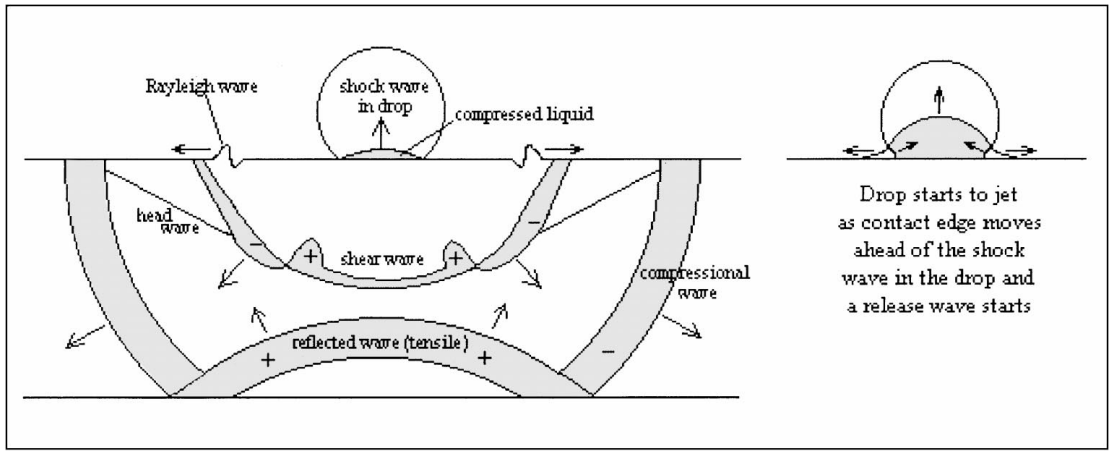

Figure A1 Impact of a spherical drop on a material showing the shock wave in the drop and the stress waves in the material. The shaded width of the shear and compressional waves represent the relative amplitudes of particle motion [34].

The pressures at the contact periphery are somewhat higher and reach approximately $3\rho_1 C_1 V$ at the instant the shock envelope overtakes the contact periphery and starts to move up the fee surface of the drop [27]. Due to the very short duration of this pulse, a few ns, these 'edge' pressures are usually ignored.

The water hammer pressures are generated over a radius of contact given by

$$R = \frac{rV}{C_1} \tag{A3}$$

where r is the radius of curvature of the drop (liquid mass) in the region of contact. Pressure release commences after a time of

$$\tau = \frac{rV}{2C_1^2}. \tag{A4}$$

The release waves reach the central axis and terminate the high-pressure stage after a time

$$\tau' = \frac{3rV}{2C_1^2}. \tag{A4}$$

Once incompressible stream line flow is established, the pressure on the central axis falls to the much lower Bernoulli stagnation pressure

$$P_i = \frac{1}{2}\rho V^2 \tag{A5}$$

In calculating the pressures for high-velocity liquid impact, it is essential to use the appropriate shock velocity. This is related to the acoustic velocity, C_0 (ca. 1500 m/s for water) by

$$C = C_0 + kV \tag{A6}$$

where k is a constant which has a value close to 2 for water in the velocity range for V up to 1000 m/s [26].

The simulation of drop impact by jet impact relies on reproducing the local liquid-solid geometry for the all-important compressible stage of collision. The incompressible flow stages with the jet and drop will be different but at this stage the pressures are much lower. For example, the ratio of P_c/P_i for velocities $V = 50$, 100 and 500 m/s are 64, 34 and 10 respectively.

Photographic evidence for the initial shock structures and the onset of jetting have been obtained for impact with drops [30, 31] and liquid wedges [32]. Pressure measurements have been made by Rochester and Brunton [33].

Acknowledgements

CFK thanks EPSRC for a studentship. The research was supported by grants from EPSRC and DERA (Malvern). R. Marrah is thanked for his technical help.

References

1. J. E. FIELD, *Wear*, in press.
2. F. P. BOWDEN and J. H. BRUNTON, *Proc. Roy. Soc. Lond. A* **263** (1961) 433.
3. *Idem.*, Nature **181** (1958) 873.
4. C. R. SEWARD, C. S. J. PICKLES, J. E. FIELD and Z. FENG, *Diamond and Related Materials* **2** (1993) 606.
5. C. R. SEWARD, C. S. J. PICKLES, R. MARRAH and J. E. FIELD, *Proc. SPIE* **1760** (1992) 280.
6. C. R. SEWARD, C. S. J. PICKLES and J. E. FIELD, *ibid.* **1326** (1990) 280.
7. C.R. SEWARD, PhD Thesis, Cambridge University, 1992.
8. C. F. KENNEDY, PhD Thesis, Cambridge University, 1998.
9. F. P. BOWDEN and J. E. FIELD, *Proc. Roy. Soc. Lon. A* **282** (1964) 331.
10. E. J. COAD, C. S. J. PICKLES, C. R. SEWARD, G. H. JILBERT and J. E. FIELD, *ibid.* **454** (1998) 213.
11. C. R. SEWARD, C. S. J. PICKLES, E. J. COAD, M. WATT and J. E. FIELD, Contract SPC-92-4032, European Office of Aerospace Research and Development, 1994.
12. R. J. HAND, J. E. FIELD and D. TOWNSEND, *J. Appl. Phys.* **70** (1991) 7111.
13. D. G. RICKERBY, PhD Thesis, Cambridge University, 1976.
14. J. E. FIELD, D. A. GORHAM, J. T. HAGAN, M. J. MATTHEWSON, M. V. SWAIN and S. VAN DER ZWAAG, in "Proceedings of the 5th International Conference on Erosion by Liquid and Solid Impact, Paper B," edited by J. E. Field (Cambridge, 1979).
15. B. STEVERDING and S. H. LEHRIGK, *Int. J. Fract. Mech.* **5** (1969) 369.

16. J. E. FIELD, S. VAN DER ZWAAG and D. TOWNSEND, in Proceedings of the 6th International Conference on Erosion by Liquid and Solid Impact, Paper N21, 1983.
17. H. KOLSKY, "Stress Waves in Solids" (Oxford University Press, 1953).
18. R. W. DAVIDGE, "Mechanical Behaviour of Ceramics" (Cambridge University Press, 1979).
19. J. E. FIELD, *Contemp. Phys.* **24** (1983) 439.
20. J. J. CAMUS., PhD Thesis, Cambridge University, 1971.
21. J. E. FIELD and M. B. LESSER, *Proc. Roy. Soc. Lond. A* **357** (1977) 143.
22. N. K. BOURNE, T. OBARA and J. E. FIELD, *ibid.* **452** (1996) 1497.
23. G. I. TAYLOR, *ibid.* **201** (1950) 192.
24. R. J. HAND, PhD Thesis, Cambridge University, 1987.
25. S. VAN DER ZWAAG, PhD Thesis, University of Cambridge, 1981.
26. F. J. HEYMANN, *J. Appl. Phys.* **40** (1969) 511.
27. M. B. LESSER, *Proc. Roy. Soc. Lon. Ser. A* **377** (1981) 289.
28. M. B. LESSER and J. E. FIELD, *Ann. Rev. Fl. Mech.* **15** (1983) 97.
29. S. S. COOK, *Proc. Roy. Soc. Lond. A* **119** (1928) 481.
30. J. P. DEAR and J. E. FIELD, *J.Appl. Phys.* **63** (1988) 1015.
31. J. E. FIELD, J. P. DEAR and J. E. ONGREN, *ibid.* **65** (1989) 533.
32. J. E. FIELD, M. B. LESSER and J. P. DEAR, *Proc. R. Soc. Lond. A* **401** (1985) 225.
33. M. C. ROCHESTER and J. H. BRUNTON, in "Proceedings of the 5th International Conference on Erosion by Liquid and Solid Impact, Paper 6," edited by J. E. Field (Cambridge, 1979).
34. R. G. WOODS, *J. Soil Mech. Founds. Div., Am. Soc. Civ. Engrs.* **94** (1968) 951.

Received 27 August 1999
and accepted 7 February 2000